Dynamics adsorption of the enhanced CH_4 recovery by CO_2 injection

Min Gu [a*] Shuo Duan [a,b] Qirong Wu [c]

(a. State Key Laboratory of Coal Mine Disaster Dynamics and Control, College of Resources and Environmental Science, Chongqing University, Chongqing 400044, China;
b. School of Mining and Geomatics, Hebei University of Engineering, Handan, Hebei, 056038, China;
c.SPIC (State Power Investment Corporation) Yuanda Environmental Protection Engineering Co., Ltd., Chongqing 400012, China)

ABSTRACT

The dynamic adsorption isotherms of CO_2-EGR were measured by using a Intelligent Gravimetric Analysis system. In the beginning stage of CO_2 injection, all the injected CO_2 enters into the adsorbent and the mole fraction of CH_4 (y_{CH4}) keeps 1.0. The CH_4 recovery factor (R_{CH4}) increases. The during of this stage (t_{cd}) depends on the selectivity of CO_2 over CH_4 ($S_{CO2/CH4}$). A adsorbent with large $S_{CO2/CH4}$ has long t_{CD}. When $S_{CO2/CH4}$ is greater than 1.0, CO_2 reduces the fraction of CH_4 in the adsorbed phase (x_{CH4}) and more CH_4 is driven out. In the second stage, the injected CO_2

* Corresponding author
E-mail address: mgu@cqu.edu.cn

competes with CH_4 for adsorption. The cumulative R_{CH4} of this stage is much larger than that of the initial stage. However, y_{CH4} decrease sharply. p_{CH4} in the whole CO_2 injection is always larger than that before CO_2 injection, suggesting CH_4 desorption results from the displacement by CO_2 rather than from pressure depletion.

Keywords : dynamic adsorption; CO_2-EGR; CH_4 displacement; the CH_4 recovery factor (R_{CH4})

1 Introduction

In the adsorption separation of mixed gas and energy extraction of conventional natural gas, CO_2 injection is being considered to improve the recovery of CH_4. For example, CO_2 injection has been proposed to use as a displacement step of PSA (pressure swing adsorption) cycle in the separation of coal-bed gas extracted (CH_4/N_2 mixture gas) using grain activated carbon (GAC) as adsorbent [1]. And CO_2 injection has also been proposed to enhance shale gas recovery (CO_2-ESGR) [2,3] and coalbed methane recovery(CO_2-ECBM) [4]. In fact, the adsorption principle of all these CO_2-enhance gas recovery (CO_2-EGR) processes is the same, that is, CO_2 can displace adsorbed CH_4 in the adsorbent/reservoir and drive out CH_4. However, these processes have not been fully understood and have not been applied in the field except several test fields.

Because most CH_4 in the adsorbent/reservoir is adsorbed state, the effect of CO_2-EGR depends largely on the competitive adsorption of CO_2 and CH_4. Shale and coal are adsorbents because they are porous material. An adsorbent has selectivity for gas

adsorption and the adsorption capacity of different gases on an adsorbent is different. The adsorption selectivity mainly depends on the the properties of the adsorbent and the adsorbed gas. The pore structure and surface properties of adsorbent and the molecular size of adsorbed gas play an important role in the adsorption selectivity [5,6]. The dynamics diameter of CO_2 molecular is 0.33nm, which is less than 0.38nm of CH_4, so it can enter the smaller pores that methane cannot enter. Therefore, the adsorption capacity of CO_2 is always greater than that of CH_4 on most adsorbents having micropores. The adsorption selectivity of CO_2 over CH_4 ($S_{CO2/CH4}$) is often used to evaluate the CO_2/CH_4 competitive adsorption [7]. The $S_{CO2/CH4}$ can be simply expressed as the ratio of the adsorption capacity of CO_2 to CH_4. In most cases, $S_{CO2/CH4}$ is calculated by the parameters of the adsorption equation of gases[5]. Numerous work were performed to get the adsorption isotherms of CO_2 and CH_4 on activated carbon adsorbent [1,8], some new adsorbent used for the separation CO_2 and CH_4[9] , coal[10] and shale reservoirs [11,12] and establish adsorption isotherm equations. $S_{CO2/CH4}$ is larger than 1.0, indicating the feasibility of CO_2-EGR.

The temperature and pressure studied for adsorption are mostly far away from the supercritical point of CH_4 (pressure 4.59 MPa, temperature -82.6 °C). On the contrary, they may close to the supercritical point of CO_2 (pressure 7.38 MPa, temperature 31.26 °C). Therefore, CH_4 adsorption isotherm curves show a linear increase followed by a plateau [1,3,5,8-12], which can be described well by Langmuir equation. Typical CO_2 adsorption isotherm consists of linear increase in gas adsorption with pressure followed by a plateau or saturation region and finally

decrease in a non-linear way on various rank coals, shale and activated carbon[1,3,8-12]. The adsorption saturation of CO_2 appears near to its supercritical point. The shape of adsorption isotherms of CO_2 vary greatly at different range of temperature and pressure, which are described by different adsorption isotherm equations, such as Langmuir equation, BET(Brunauer-Emmett-Teller) equation and Virial equation et.al. However, all the adsorption works describe adsorption equilibrium of CH_4 and CO_2 from thermodynamic view. Some study the kinetic adsorption to compared the diffusion coefficient of CO_2 and CH_4[3,3-15]. However, these adsorption thermodynamic and adsorption kinetic have not reflected the dynamic adsorption process of CO_2 injection to adsorbent adsorbed CH_4.

CO_2-EGR is a dynamic process in which CH_4/CO_2 competitive adsorption is always changing with CO_2 injection. The core flooding test (fixed bed experiment) is a directly experimental method to simulate the dynamic process [1-4,16], whose results are breakthrough curves of CO_2 and CH_4. By fitting the breakthrough curves using numerical models consist of the material balance equations, adsorption equations and mass transfer equation, the CH_4 recovery factor (R_{CH4}), the cumulative CH_4 production and CO_2 storage amount are obtained[1]. In addition, the transport properties of CO_2 in adsorbents can be obtained by using some hydrodynamic models[2,16], permeability and porosity evolution models[17].

In this paper, we obtained the dynamic adsorption isotherms of the whole CO_2-EGR process by conducting an experiment. The dynamic adsorption mechanisms of CO_2-EGR were analyzed based on the dynamic adsorption isotherms. Moreover, the

CH_4 recovery factor (R_{CH4}) of CO_2-EGR were also obtained. The CO_2-EGR process was simulated by injecting CO_2 into the adsorbents that pre-adsorbed CH_4 and were conducted on the intelligent Gravimetric Analysis system (IGA 100B) with scale of 200 mg. Because the amount of adsorbent that can be filled in sample basket of the IGA 100 equipment is less than 200mg, the adsorbent chosen should have a large adsorption capacity for CH_4 and CO_2 to reduce the fitting error of the adsorption curve. The specific surface area of shale and coal is much smaller than that of activated carbon, therefore, activated carbon are used instead of shale or coal sample.

2 Experimental

2.1 Materials

Activated carbons of CF-30 (prepared in our laboratory [5]) and RX3 (Norit Netherland B.V.) were used in the experiments. The BET (Brunauer-Emmett-Teller) surface area (S_{BET}) and the pore size distribution (PSD) of CF-30 and RX3 were determined by ASAP2020 apparatus (Micromeritics, USA). The measured S_{BET} of CF-30 and RX3 are 426.49 m^2/g and 1238.20 m^2/g, respectively. The PSDs of the two GACs are shown in Fig. 1, which show that the pores of CF-30 are mainly contributed by micropores (pore size<20 Å, 2nm). The RX3 has both micropores and many mesopores (20-500 Å, 2-5nm).

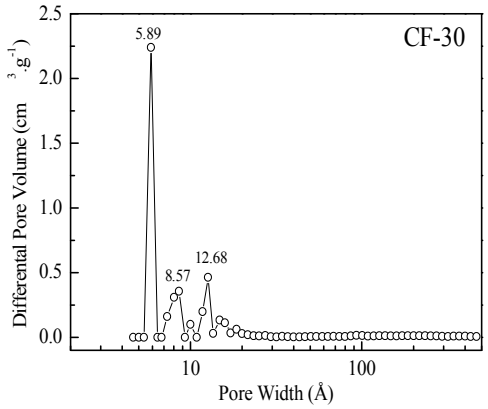

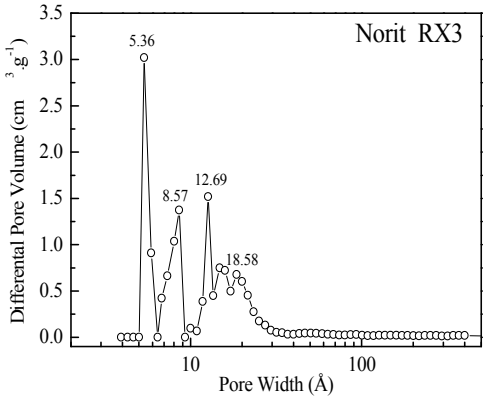

Fig.1. The pore size distributions of CF-30 and RX3.

The purities of CH_4 and CO_2 were 99.995% and 99.999%, respectively, as stated by the supplier Tianke Co. China. The estimated uncertainty of the adsorption

measurements due to gas purity was negligible.

2.2 Adsorption measurement

Intelligent Gravimetric Analysis (IGA) apparatus can determine accurately the increase of the weight of the adsorbent due to the adsorption of the gas. The IGA-100B used in this paper apparatus is manufactured by Hiden Isochema, Ltd. (UK) with a weight resolution of 0.2 mg.

The equilibrium adsorption isotherms of CH_4 and CO_2, and the dynamic adsorption isotherms of CO_2-EGR process were measured at 298K on IGA-100B apparatus.

3 Results and discussion

3.1 The selectivity of CO_2 over CH_4

3.1.1 Adsorption isotherms of CH_4 and CO_2

The adsorption isotherms of CH_4 and CO_2 on GACs are shown in Fig.2. It is obviously that adsorption amount of CO_2 is larger than CH_4, meaning that the preferential adsorption of CO_2 over CH_4.

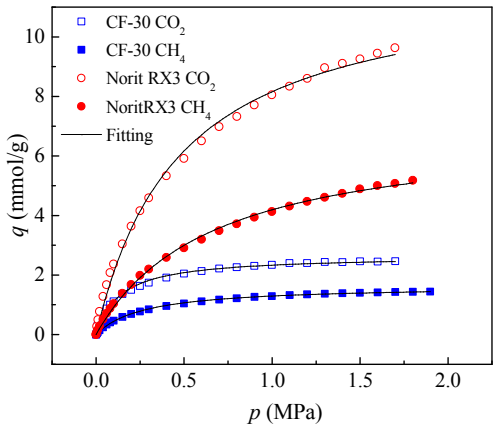

Fig.2. Adsorption isotherms and Langmuir fitting curve of CH_4 and CO_2 on CF-30 and RX3 GACs

The shape of each of these isotherms fall into Type I in the IUPAC classification [5], single-gas Langmuir equation (Eq. 1) is used for the simulation of these isotherms.

$$q_i = \left(\frac{q_{mi} b_i p}{1 + b_i p} \right) \tag{1}$$

where q_i(mol/g), q_{mi} (mol/g) and b_i are the adsorption amount, maximum adsorption capacity and adsorption equilibrium constant of pure gas i, respectively; p is the equilibrium pressure.

The fitting parameters of Eq.(1) for the adsorption isotherms of CH_4 and CO_2 are listed in Table 1. High values of correlation coefficient (R) indicate that Eq.1 describes these isotherms well. However, there are still some errors between adsorbed amount measured and predicted by Eq.(1). The relative errors of adsorbed amount for CH_4 are less than 2% on both GACs at all pressures. It is noted that the CO_2 predictions at pressures lower than 0.15MPa show negative relative errors for RX3, but positive for CF-30.

Table1 Langmuir equation fitting parameters for CH_4 and CO_2

Adsorbent	CH_4			CO_2		
	q_{mCH4} (mmol/g)	b_{CH4} (MPa^{-1})	R^2	q_{mCO2} (mmol/g)	b_{CO2} (MPa^{-1})	R^2
CF-30	1.65	3.66	0.999	2.65	7.24	0.997
RX3	6.96	1.51	0.999	12.04	2.10	0.998

A higher b indicates a higher affinity of the adsorbent for the adsorbate. The b values of CO_2 (b_{CO2}) are larger than those of CH_4 (b_{CH4}) for both GAC samples, suggesting that the interaction forces of CO_2-GAC are larger than those of CH_4-GAC. Moreover, CF-30 has much stronger affinity for CO_2 than RX3.

3.1.2 The adsorption selectivity of CO_2 over CH_4

$S_{CO2/CH4}$ can be calculated by Eq. (2) [3,5] for gases adsorption isotherms follow the adsorption isotherm of Langmuir equation ,

$$S_{CO_2/CH_4} = \frac{x_{CO_2} / y_{CO_2}}{x_{CH_4} / y_{CH_4}} = \frac{q_{mCO_2} \cdot b_{CO_2}}{q_{mCH_4} \cdot b_{CH_4}} \quad (2)$$

where x_{CH4} and x_{CO2} are the mole fractions of component CH_4 and CO_2 in adsorbed-phase, respectively; y_{CH4} and y_{CO2} are the mole fractions of CH_4 and CO_2 in the gas-phase respectively. The b and q_m of CH_4 and CO_2 are listed in Table1.

$S_{CO2/CH4}$ of CF-30 is 3.19 and of RX3 is 2.41. $S_{CO2/CH4}$ greater than unity implies that CO_2 is a greater affinity of CO_2 over CH_4, and the process of enhanced CH_4 by CO_2 can be feasible from the thermodynamic point of view. The pores of carbonaceous materials are usually slit-shape. The minimum widths of the slit like pores for CO_2 and CH_4 molecules entering are 0.578 nm and 0.62 nm, respectively[18]. That is one reason why $S_{CO2/CH4}$ is always greater than unity for most adsorbents having micropores. Moreover, the adsorption energy ratios of CO_2/CH_4 in the slit-shape pores size range from 0.62 to 1.6 nm decreases from 2.1 to 1.06 [18]. Therefore, only smaller size micropores have larger selectivity for small molecules of CO_2 and CH_4[5,9,18]. In

the pores larger than 1.6 nm, the competitive adsorption between CO_2 and CH_4 is weak. Because RX3 activated carbon has much more pores larger than 1.6nm, the percentage of the pores whose size less than 1.6nm in CF-30 is larger than in RX3, the $S_{CO2/CH4}$ of CF-30 is larger than that of RX3.

3.1.3 The distribution of CO_2 and CH_4 in the adsorbed and gas phase at equilibrium state

At an equilibrium state, the mole fraction of CH_4 in adsorbed phase (x_{CH4}) is related to that in gas phase (y_{CH4}) by $S_{CO2/CH4}$, which is [19]

$$\frac{1}{x_{CH_4}}=\frac{S_{CO_2/CH_4}}{y_{CH_4}}+\left(1-S_{CO_2/CH_4}\right) \qquad \frac{1}{x_{CH_4}}=\frac{S_{CO_2/CH_4}}{y_{CH_4}}+\left(1-S_{CO_2/CH_4}\right) \tag{3}$$

Combined with Eq.(4) and Eq.(5), the correlations of x_{CH4}-y_{CH4} and x_{CO2}-y_{CO2} are decided and are shown in Fig.4.

$$y_{CH_4}+y_{CO_2}=1 \tag{4}$$

$$x_{CH_4}+x_{CO_2}=1 \tag{5}$$

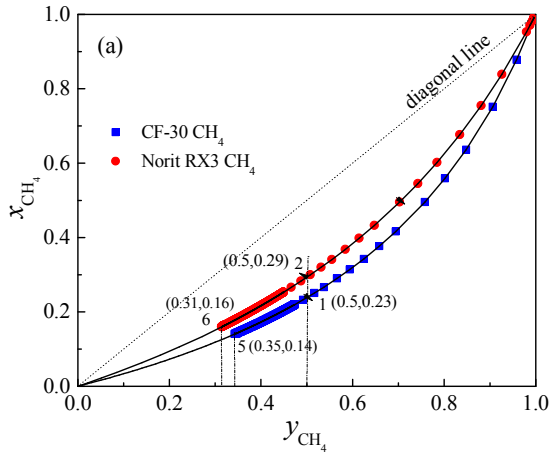

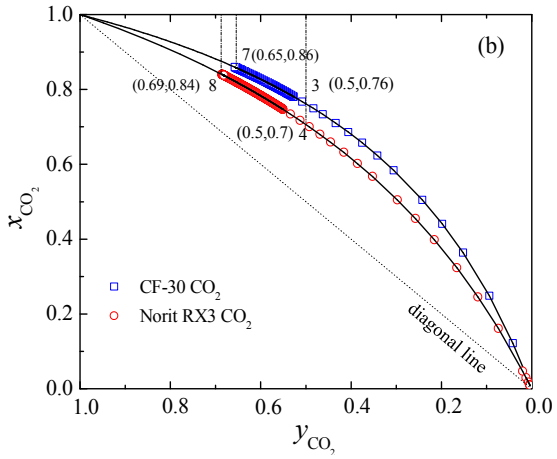

Fig. 3. The relationships x_{CH4}-y_{CH4} (a)and x_{CO2}-y_{CO2} for CF-30 and RX3(b).

If there is no adsorption competition between two gas components i and j , the adsorption selectivity of CO_2 over CH_4 ($S_{i/j}$) is 1.0. Hence, the correlations of x.y are

straight diagonal line, as shown as dot lines in Fig 3. On the contrary, any deviation from the diagonal *x*-*y* line means the occurrence of adsorption competition. For CH_4 adsorption shown in Fig.3a, x_{CH4}-y_{CH4} curves locate below the diagonal line, indicating that the CO_2 hinders CH_4 adsorption and reduces fractions of CH_4 in adsorbed-phase (x_{CH4}). This is why CH_4 displacement by CO_2 is possible for $S_{CO2/CH4}>1$. For example, at the same y_{CH4} values of 0.5, x_{CH4} for CF-30 and RX3 is 0.23 (point 1) and 0.29 (point 2), respectively. Moreover, x_{CH4} decreases much with a large $S_{CO2/CH4}$. On the contrary, x_{CO2}-y_{CO2} of CO_2 adsorption curves in Fig.3b locate above diagonal line. x_{CO2} increases much with a large $S_{CO2/CH4}$. For example, x_{CO2} is 0.76 for CF-30 and is 0.7 for RX3 when y_{CO2} is 0.5, as shown by point 3 and point 4 in Fig.3b. It is concluded that more relative CH_4 molecules are driven out and the mole fraction of CO_2 is higher in the adsorbent with high $S_{CO2/CH4}$.

3.2 The adsorption dynamic of CO_2-EGR

3.2.1 The adsorption dynamic isotherms of CO_2-EGR

The dynamic adsorption isotherms (q_t-t) and their corresponding pressure histories are shown in Fig.4. AC stage of the q_t-t curve corresponds to the adsorption of CH_4. In the AB stage, the pressure increased from 0.0 MPa to 0.1 MPa, and the adsorption amount of CH_4 increased from 0.0 mg/g to 6.1mg/g. Then in the BC stage, the pressure is kept at 0.1 MPa for about 20min to reach the equilibrium state of CH_4 adsorption. The CF phase corresponds to CO_2 injection process after CH_4 pre-adsorption. The pressure is increased from 0.1 MPa to 0.3 MPa (CE phase) and maintained at 0.3 MPa for about 46min to reach an adsorption equilibrium (EF phase).

The adsorption amount (q_t) is the total adsorption amount of CH_4 and CO_2, which reflects the adsorption competitive change CO_2-CH_4 with CO_2 injection. In the CE phase, p-t is a line, while q_t-t is not a line.

The q-t curves obtained by using shale sample is exactly the same as that shown in Figure 4. We chose the results of GAC adsorbent to analyses the dynamic adsorption process, because the GAC has a much larger adsorption amount than shale, and hence the error in the numerical simulation is smaller.

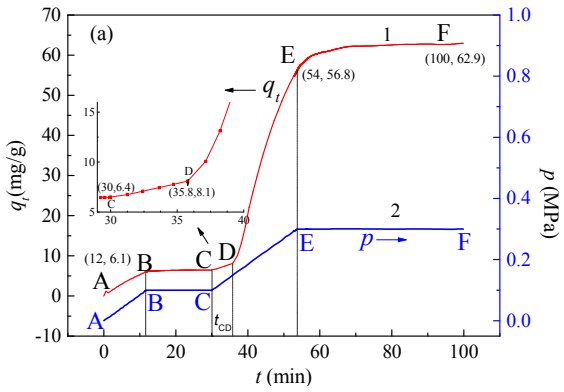

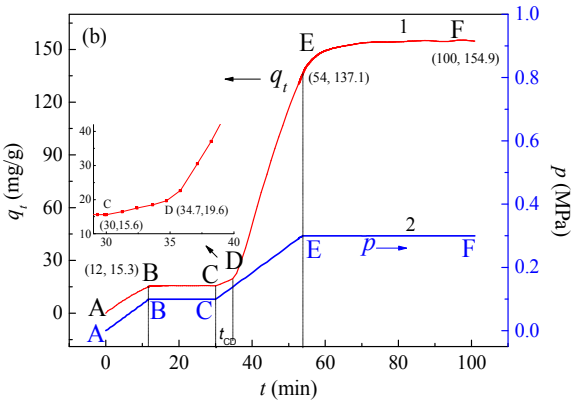

Fig. 4. Adsorption dynamic isotherms and pressure history of the CO_2-EGR in different adsorbents (a) CF-30; (b) RX3

The slope of CD segment is much smaller than that of DE segment, which indicates that the adsorption capacity in CD phase increases little, but the adsorption capacity increases sharply in DE process. Moreover, the time for CD stage (t_{CD}) is much shorter than the time for DE stage (t_{DF}). As shown in Fig.4, the t_{CD} is 5.8min and 4.7min; t_{DF} is 18min and 19.3 min for CF-30and RX3, respectively.

3.2.2 The mole fractions of CH_4 and CO_2 in the gas phase of CO_2-EGR

The co-adsorption isotherms of CO_2/CH_4 binary mixtures on both of the GACs can be well fitted by multi-component Langmuir equations, Eq.6 and Eq.7, [5]

$$q_{CH_4}=\frac{q_{mCH_4}b_{CH_4}py_{CH_4}}{1+b_{CH_4}py_{CH_4}+b_{CO_2}p(1-y_{CH_4})} \quad (6)$$

$$q_{CO_2}=\frac{q_{mCO_2}b_{CO_2}p(1-y_{CH_4})}{1+b_{CH_4}py_{CH_4}+b_{CO_2}p(1-y_{CH_4})} \quad (7)$$

where p is total pressure, q_{CH4} and q_{CO2} (mol/g) are the adsorption amounts of

components CH_4 and CO_2 from a binary gas mixture, respectively. q_{mCH4}, b_{CH4}, q_{mCO2} and b_{CO2} are the Langmuir parameters of pure CH_4 or CO_2 listed in Table 1. y_{CH4} and y_{CO2} are CH_4 and CO_2 in the gas-phase respectively.

In the process of CO_2 injection, the adsorption amount q_t is the total adsorbed amount of CH_4 and CO_2. q_t is expressed by weight (mg / g) as Eq. (8).

$$q_t = q_{CH_4} M_{CH_4} + q_{CO_2} M_{CO_2} \tag{8}$$

where q_{CO2} (mmol/g) and M_{CO2} (44g/mol) are the adsorbed amount and molecular weight of CO_2, respectively; q_{CH4} (mmol/g) and M_{CH4} (16g/mol) are the adsorbed amount and molecular weight of CH_4, respectively.

The mole fraction of CH_4 (y_{CH4}) at different pressure is calculated by Eq. which is derived from Eq.6 combined with Eq. 8. Combined with *p-t* curve, the curve of CH_4 concentration in the gas phase with time (y_{CH4}-*t*) during CO_2 injection is obtained, as shown in Fig. 5a. y_{CO2} is calculated by Eq. (4), and y_{CO2}-*t* is shown in Fig. 5b.

$$y_{CH_4} = \frac{q_{mCO_2} b_{CO_2} p M_{CO_2} - b_{CO_2} q_t p - q_t}{p(b_{CH_4} q_t - b_{CO_2} q_t - M_{CH_4} b_{CH_4} q_{mCH_4} + M_{CO_2} b_{CO_2} q_{mCO_2})} \tag{9}$$

It is obviously that there are two stages (CD and DE) before y_{CH4} and y_{CO2} reaches a constant value. In the initial stage (CD stage) of CO_2 injection process, y_{CH4} keeps a constant about 1.0. In CD stage, y_{CH4} should be 1.0 theoretically. There is a little deviation between the calculated y_{CH4} and 1.0, which is due to the error in the prediction of CO_2 and CH_4 adsorption capacity in Eq. (1), which has been discussed in 3.1.1.

y_{CH4}-*t* curves reflect the time evolution of the the effluent composition, as the

same as breakthrough curves obtained by core flooding tests. The patterns of y_{CH4}-t shown in Fig.5a are in agreement with all the CH_4 breakthrough curves obtained in the CO_2 injection process for enhancing gas shale[2,16,17], coal bed gas[4] and for enriching CH_4 in separation for CH_4/N_2[1] by PSA experiments. In all the breakthrough curves, y_{CH4} remained at 1.0 at the beginning of CO_2 injection. CO_2 breakthrough at D, and the second DE stage begins. y_{CH4} deceases dramatically in this stage. It is should be noted that in the whole CO_2 injection process, the duration of the initial stage t_{cd} is very short. The early breakthrough of CO_2 was also found in in CO_2-ESGR and CO_2-ESGR (CO_2-ECBM) [1-3,16,17], which was unfavorable for CH_4 production. The CH_4 product is contaminated by CO_2 after CO_2 breakthrough. For the PSA separation, the time length of CO_2 displacement step must shorter than t_{cd}.

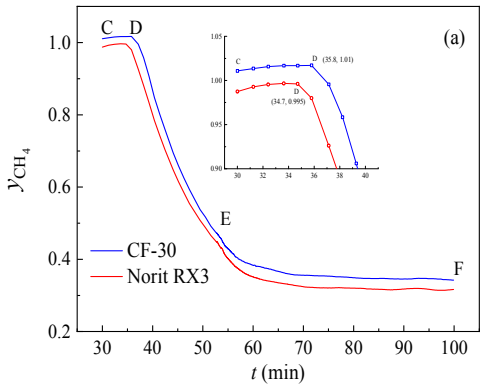

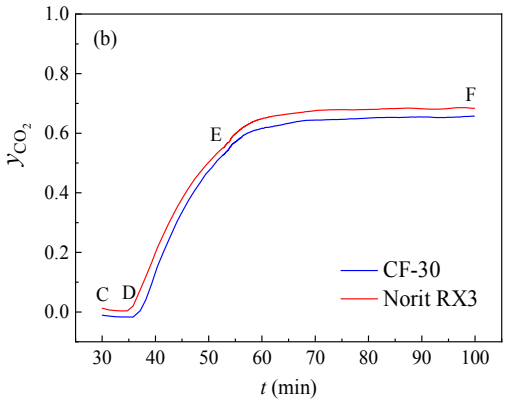

Fig. 5. The time evolution of the mole fraction of CH_4 (a) and CO_2 (b) in the gas phase with CO_2 injection

3.2.3 The partial pressure of CO_2 and CH_4 of CO_2-EGR

The absolute partial pressure of CH_4 (p_{CH4}) and CO_2 (p_{CO2}) in the gas phase are calculated according to Eq.10 and Eq.11, in which p is the total pressure shown in Fig.1. The calculated results of p_{CH4}-t and p_{CO2}-t curves are shown in Figure 6. p_{CO2} deviates a little bit from 0.0 in the CD stage, and p_{CH4} deviates a little bit from 1.0 at C point, which are also due to the fitting error of Langmuir equation(as discussed in 3.1.1).

$$p_{CH4}=p\,y_{CH4} \quad (10)$$

$$p_{CO2}=py_{CO2}=p\,(1-y_{CH4}) \quad (11)$$

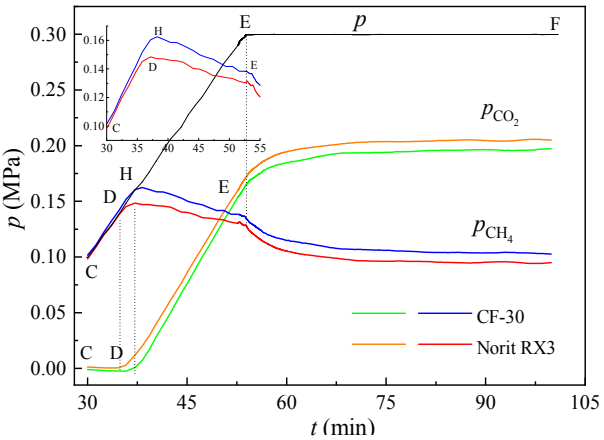

Fig.6 The change of p_{CH4} and p_{CO2} with time in the process of CO_2 injection

In the CD stage of CO_2 injection, p_{CH4} raises sharply with the CO_2 injection; while p_{CO2} keeps zero. It is should be noted that p_{CH4} is always higher than that before CO_2 injection (0.1MPa). This results show that CH_4 absorption always occurs in the CO_2 injection process. p_{CH4} still increases for a little time after CO_2 breakthrough. This is because the total pressure p increased, although y_{CH4} decreases. Then, p_{CH4} decreases, but p_{CO2} increases dramatically. At the EF stage, p_{CH4} and p_{CO2} reach a constant value gradually under the maintain pressure of 0.3 MPa.

3.3.4 The CH_4 recovery factor of CO_2-EGR

Because the pressures of the gas are low, the equation of state (EOS) for an ideal gas can be used,

$$pV = nRT \tag{12}$$

where V is the volume, p is the partial pressure of gas, R is the gas constant, n is number of moles and T is the temperature.

Let p_1 and n_1 be the partial pressure and number of moles of CH_4 before CO_2

injection, p_2 and n_2 be the partial pressure and number of moles of CH_4 after CO_2 injection. And hence (n_2-n_1) is the CH_4 displacement amount by CO_2. Their relationship of p and n is given by Eq.(13). The CH_4 recovery factor (R_{CH4}) is given by Eq.(14).

$$\frac{p_2}{p_1}=\frac{n_2}{n_1} \tag{13}$$

$$R_{CH_4}\%=\frac{n_{2\,CH_4}-n_{1\,CH_4}}{n_{1\,CH_4}}\times 100\%=\left(\frac{n_{2\,CH_4}}{n_{1\,CH_4}}-1\right)\times 100\%=\left(\frac{p_{2\,CH_4}}{p_{1\,CH_4}}-1\right)\times 100\% \tag{14}$$

The calculated R_{CH4} with time is shown in Figure 7, which show that R_{CH4} raises rapidly in the CD stage, and then declines rapidly in the HE stage. R_{CH4} decreased slowly in EF, and then reached a stable value. The results are consistent with the shale gas analysis results [20].

In the CD phase, R_{CH4} of CF-30 and RX3 increased to 51.02% and 35.75%, respectively. The accumulation of R_{CH4} in CF-30 is 1.7 times that of RX3. This is because the CF-30 has more small pores which only CO_2 can enter into. It is noted that the peaks of R_{CH4} and p_{CH4} did not appear in the initial stage of CD. The maximum values of R_{CH4} are 61.1% and 47.6% which appear at H point of DE stage, and the corresponding y_{CH4} are 0.95 and 0.92, respectively. Wang [20] also noted that the peak productivity would not appear in the first month. At the end of DE phase, R_{CH4} decrease to 36.1% and 27.7%, and y_{CH4} is 43.9% and 41.8% in CF-30 and RX3, respectively. In DE stage, the cumulative R_{CH4} value of CF-30 is 1.23 times that of RX3. In addition, the accumulation of R_{CH4} in DE stage was much higher than that in

CD stage. The cumulative R_{CH4} of CF-30 and RX3 in DE phase are 63.1 and 86.5 times of that in CD phase, respectively. With the increase of cumulative R_{CH4}, y_{CH4} decreases after CO_2 breakthrough at D point. At the equilibrium stage (EF), the R_{CH4} is very small. As seen from Fig. 5, at point F of the equilibrium stage (EF), y_{CH4} of CF-30 and RX3 are 0.35 and 0.31, which result show that more CH_4 is displaced to the gas phase on CF-30 than on RX3. As shown in Fig.3a, y_{CH4} of 0.35 corresponds to x_{CH4} of 0.14 (point 5) for CF-30, and y_{CH4} of 0.31corresponds to x_{CH4} of 0.16 (point 6) for RX3.These results show that the residual CH_4 in RX3(x_{CH4} of 0.16) is more than that in CF-30(x_{CH4} of 0.14). Therefore, a larger $S_{CO2/CH4}$ results in a larger R_{CH4}.

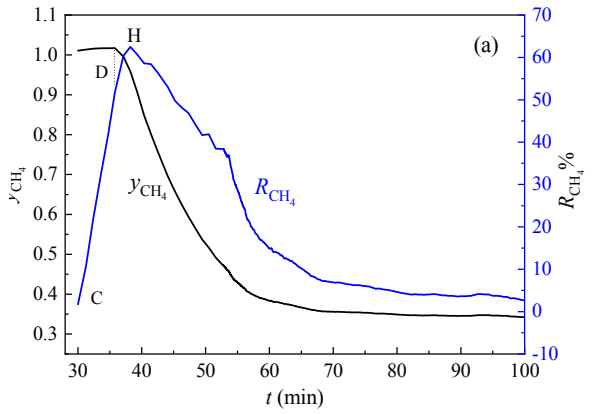

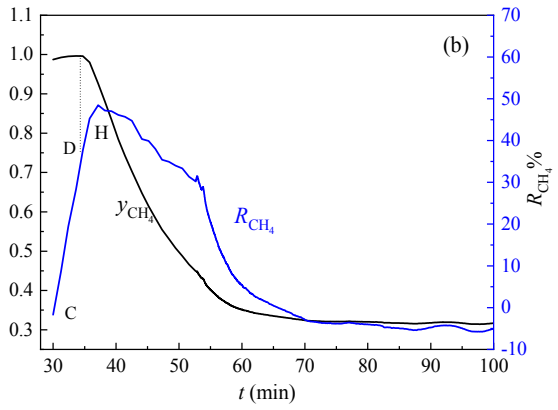

Fig.7 The time evolution CH_4 recovery (R_{CH4}) and y_{CH4} during CO_2 injection

3.3 The dynamic adsorption mechanism of CO_2-EGR

The dynamic curves of the q_t, y_{CH4}, p_{CH4} and p_{CO2} with time demonstrate that there are two adsorption stages during the continue CO_2 injection before adsorption equilibrium. These two stages also appear in the breakthrough curves[1-3] and the permeability curve with time in other studies[17]. The duration of the initial CO_2 injection stage(t_{CD}) relies on the selectivity of CO_2 over CH_4 ($S_{CO2/CH4}$). A larger $S_{CO2/CH4}$ of an adsorbent (reservoir) have longer t_{CD} and high R_{CH4} in the CO_2 injection process.

In the initial CO_2 injecting (CD stage), p_{CO2} keeps zero, suggesting that all the CO_2 injected enters into adsorbent. Both of the CF-30 and RX3 GACs have many pores whose size is less than 0.62 nm, where CO_2 can enter into, but CH_4 is inhibited. Moreover, CO_2 is adsorbed some surface sites larger than 0.62nm where have not been occupied by CH_4. The entering of CO_2 reduces the CH_4 partial pressure in the adsorbent, and hence CH_4 desorbs and enters the gas phase. The desorption rate of CH_4 and R_{CH4} rate are fast because no competitive adsorption occurs.

In the DE stage of CO_2 injection, CO_2 enters into adsorption sites where CH_4

have occupied and competitive adsorption between CH_4 and CO_2 occurred. Once competitive adsorption occurs, CO_2 mixes with CH_4 .Therefore, the desorption gas is a mixture of CH_4/CO_2, which is confirmed by the y_{CH4} less than1.0. Because of the continue CH_4 desorption, more pores are left and more CO_2 is adsorbed. The cumulative R_{CH4} of the initial stage are much larger than that of the initial stage, confirms that most CH_4 in the adsorbent as adsorbed state.

p_{CH4} is always larger than 1.0 MPa in the whole CO_2 injection. It is suggested that CH_4 desorption is not by the gas phase pressure depletion. According to the common sense, CH_4 should be adsorbed rather than desorbed when the CH_4 partial pressure in the gas phase increases. However, CH_4 always desorption during CO_2 continue injection, which confirms the strong adsorption and displacement capacity of CO_2. p_{CH4} and R_{CH4} raise with high rate in the CD stage of CO_2 injection. More important, y_{CH4} keeps 1.0 only in the CD stage and then declines a lot. The CD stage of CO_2 injection is ideal for the CO_2-EGR. The CH_4 product is pure, R_{CH4} rate increases. An adsorbent with large $S_{CO2/CH4}$ has long t_{CD}.

4 Conclusions

The results in this paper presented a better understanding of the dynamic adsorption mechanism of gas recovery by CO_2 injection(CO_2-EGR). CO_2-EGR experiment was contacted by the continuous injection of CO_2 into the adsorbent pre-adsorbed with CH_4.

(1) The adsorption selectivity of CO_2 over CH_4 ($S_{CO2/CH4}$) is an important

parameter that evaluates the possibility and effectiveness of the CO_2-EGR. When $S_{CO2/CH4}$ is larger than 1.0, CO_2 hinders CH_4 adsorption and reduces fractions of CH_4 in adsorbed-phase (x_{CH4}). The adsorbent with more micropore size has larger $S_{CO2/CH4}$. More CH_4 molecules will be driven out from the adsorbent of high $S_{CO2/CH4}$.

(2) The adsorption dynamic isotherms of CO_2-EGR were measured. There are two adsorption stages in CO_2 injection process. At the beginning of CO_2 injection (CD stage), all of the injected CO_2 is adsorbed in the adsorbent and p_{CO2} keeps zero. p_{CH4} and R_{CH4} raise fast. This stage is the ideal period for CO_2-EGR. The during of this stage (t_{cd}) depends on $S_{CO2/CH4}$. A large $S_{CO2/CH4}$ has a longer t_{cd}.

(3) In the second stage, the cumulative R_{CH4} is much larger than that of the CD stage, confirming that most CH_4 was desorbed is driven out at this stage. The injected CO_2 enters the adsorption site occupied by CH_4, competes with CH_4 for adsorption, and mixes with CH_4. The gas released from the adsorbent is CH_4/CO_2 mixture. p_{CO2} increase and y_{CH4} decreases sharply.

(4) p_{CH4} in the whole CO_2 injection is always larger than that before CO_2 injection, suggesting CH_4 desorption results from the displacement by CO_2 rather than from pressure depletion.

AUTHOR INFORMATION

Corresponding Author E-mail: mgu@cqu.edu.cn. Phone: +86 15922640072. Fax: +86 23 65105719.

ACKNOWLEDGMENTS

This work was supported by Chongqing Science and Technology Commission Projects (grant nos. cstc2017jcyj-yszx0012, cstc2018jcyj- yszx0016, and cstc2020yszx-jcyjX0008), and Natural Science Foundation of Hebei Province (E2020402072).

REFERENCES

(1) Liu, C.; Zhou, Y.; Sun, Y.; Su, W.; Zhou, L. Enrichment of Coal-Bed Methane by PSA Complemented with CO_2 Displacement. *AIChE J*. **2011**, 57, 645-654.

(2) Du, X.; Gu, M.; Duan, S.; Xian, X. The Influences of CO_2 Injection Pressure on CO_2 Dispersion and the Mechanism of CO_2-CH_4 Displacement in Shale. *J. Energ. Resour. Technol.* **2018**, *140*, 012907.

(3) Rezlerová, E.; Brennan, J. K.; Lísal, M. Methane and carbon dioxide in dual-porosity organic matter: molecular simulations of adsorption and diffusion. *AIChE J*. **2020**, e16655.

(4) Mukherjee, M.; Misra, S. A review of experimental research on Enhanced Coal Bed Methane (ECBM) recovery via CO_2 sequestration. *Earth-Sci. Rev.* **2018**, *179*, 392-410.

(5) Gu, M.; Zhang, B.; Qi, Z.; Liu, Z.; Duan, S.; Du, X.; Xian, X. Effects of pore structure of granular activated carbons on CH_4 enrichment from CH_4/N_2 by vacuum pressure swing adsorption. *Sep. Purif. Technol.* **2015**, *146*, 213-218.

(6) Gu, M.; Xian, X.; Duan, S.; Du, X. Influences of the composition and pore

structure of a shale on its selective adsorption of CO_2 over CH_4. *J. Nat. Gas Sci. Eng.* **2017**, *46*, 296-306.

(7) First, E. L.; Hasan, M. M. F.; Floudas, C. A. Discovery of novel zeolites for natural gas purification through combined material screening and process optimization. *AIChE J.* **2014**, *60*, 1767-1785.

(8) Sudibandriyo, M.; Pan, Z. J.; Fitzgerald, J. E.; Robinson Jr., R. L.; Gasem, K. A. M. Adsorption of Methane, Nitrogen, Carbon Dioxide, and Their Binary Mixtures on Dry Activated Carbon at 318.2 K and Pressures up to 13.6 MPa. *Langmuir* **2003**, *19*, 5323-5331.

(9) Shan, B.; Yu, J.; Armstrong, M. R.; Wang, D.; Mu, B.; Cheng, Z.; Liu, J. A cobalt metal−organic framework with small pore size for adsorptive separation of CO_2 over N_2 and CH_4. *AIChE J*. **2017**, *63*, 4532-4540.

(10) Wang, Q. Q.; Zhang, D. F.; Wang, H. H.; Jiang, W. P,; Wu, X. P.; Yang, J.; Huo, P. L. Influence of CO_2 Exposure on High-Pressure Methane and CO_2 Adsorption on Various Rank Coals: Implications for CO_2 Sequestration in Coal Seams. *Energy Fuels* **2015**, *29*, 3785-3795

(11) Wang, T. Y.; Tian, S. C.; Li, G. S.; Sheng, M. Selective adsorption of supercritical carbon dioxide and methane binary, mixture in shale kerogen nanopores. *J. Nat. Gas Sci. Eng.* **2018**, *50*, 181-188.

(12) Duan, S.; Gu, M.; Du, X.; Xian, X. Adsorption Equilibrium of CO_2 and CH_4 and Their Mixture on Sichuan Basin Shale. *Energy Fuels* **2016**, *30*, 2248-2256.

(13) Du, X. D.; Gu, M.; Hou, Z.; Liu, Z.; Wu, T. Experimental Study on the Kinetics

of Adsorption of CO_2 and CH_4 in Gas-Bearing Shale Reservoirs. *Energy Fuels* **2019**, *33*, 12587-12600.

(14) Salleh, W.; Ismail, A. F. Fabrication and characterization of PEI/PVP−based carbon hollow fiber membranes for CO_2/CH_4 and CO_2/N_2 separation. *AIChE J.* **2012**, *58*, 3167-3175.

(15) Shao, X.; Feng, Z.; Xue, R.; Ma, C.; Wang, W.; Peng, X.; Cao, D. Adsorption of CO_2, CH_4, CO_2/N_2 and CO_2/CH_4 in novel activated carbon beads: Preparation, measurements and simulation. *AIChE J.* **2011**, *57*, 3042-3051.

(16) Du, X. D.; Gu, M.; Duan, S.; Xian, X. F. Investigation of CO_2-CH_4 Displacement and Transport in Shale for Enhanced Shale Gas Recovery and CO_2 Sequestration. *J. Energ. Resour. Technol*. **2017**, *139*, 012909.

(17) Xiang, L.; Elsworth, D. Geomechanics of CO_2 enhanced shale gas recovery. *J. Nat. Gas Sci. Eng.* **2015**, *26*, 1607-1619.

(18) Cui, X. J.; Bustin, R. M.; Dipple, G. Selective transport of CO_2, CH_4, and N_2 in coals: insights from modeling of experimental gas adsorption data. *Fuel* **2004**, *83*, 293-303.

(19) Gu, M.; Chen, C. G.; Xian, X. F. Adsorption characteristics of mixed gas. *Nat. Gas Ind.* **2001**, *21*, 91-93.

(20) Wang, H. What Factors Control Shale-Gas Production and Production-Decline Trend in Fractured Systems: A Comprehensive Analysis and Investigation. *SPE J*. **2017**, *22*, 562-581.